Dynamics and asymmetric behavior of loss-induced bound states in the continuum in momentum space

Qianju Song [1], Zao Yi [1,*], Hong Xiang [2,†] and Dezhuan Han [2,‡]
[1] *School of Mathematics and Physics, Southwest University of Science and Technology, Mianyang 621010, China*
[2] *College of Physics, Chongqing University, Chongqing 401331, China*

(Received 13 January 2023; revised 2 March 2023; accepted 5 April 2023; published 24 April 2023)

Bound states in the continuum (BICs) are peculiar discrete states embedded in the continuous spectrum. It has been reported that BICs still exist and exhibit new features when parity-time (PT)-symmetric perturbation is applied to the system supporting BICs. Here, we further study the PT unbalanced system, especially a purely passive one, and find that a BIC with a divergent radiative Q factor also exists when differential loss is introduced. Meanwhile, merging of two BICs is observed when varying the strength of the differential loss. Different from the ordinary BIC, this loss-induced BIC can be excited by an external plane wave, although it will not radiate to infinity. On the contrary, another mode at the same frequency but opposite wavevector can radiate, but cannot be excited by an external plane wave, manifesting the asymmetric behavior in momentum space. As the gain is introduced, the net loss can even be compensated precisely, giving rise to a PT-BICs. The Q-factor divergence rate of the PT-BICs is anisotropic in the parameter space. These results can be extended to other systems favorable for experimental implementation and may facilitate applications in light trapping and lasing.

DOI: 10.1103/PhysRevB.107.165142

I. INTRODUCTION

Bound states in the continuum (BICs) are a type of spatially localized states, although the corresponding frequencies lie inside the continuous spectrum. It was first proposed in the custom-made potential in a quantum system [1], and was then revealed to be a general phenomenon for both quantum and classical waves [2–19]. For a system containing more than one resonance and at least one open channel, BICs can be realized when the leakage via the open channel is canceled due to the destructive interference between the resonances at the open channels [2]. When the constituent open channels are the Bloch waves in the photonic crystal, BICs can be formed based on the total internal reflection of Bloch waves [4,5]. From the topological viewpoint, BICs can be interpreted by the phase singularity of the quasi-mode coupling strength for the one-dimensional chain [6,7], or the vortex centers of the polarization directions of the far-field radiation for two-dimensional photonic crystal slabs [8–14].

On the other hand, the non-Hermitian Hamiltonian has received considerable research interest recently [20–25]. When the non-Hermitian Hamiltonian possesses the combined parity-time (PT) symmetry, a PT phase transition from real to complex spectra takes place at the exceptional point [26]. Non-Hermitian optical systems with both passive and active media have been intensively investigated in recent years [27–39]. The non-Hermitian Hamiltonian offers another dimension to the original ε-μ-plane for electromagnetic metamaterials [20]. Exceptional points and nonreciprocal light transmission are extensively investigated in the two-level systems [27,28]. A lot of interesting phenomena, such as loss-induced transparency [28], unidirectional propagation [29], Bloch oscillation [30], single-mode lasing [31,32], rings of exceptional points [33], nonlinear supermodes [34], and asymmetric phase-locked states [35], are revealed in non-Hermitian systems.

Here, we study both numerically and analytically how BICs evolve when the non-Hermitian perturbation is applied to the dimerized chain. We begin with the case that common loss is introduced to two nanoparticles, A and B, in a unit cell, finding that BICs can still exist, as characterized by the divergence of the radiative Q factors. Next, the case of differential loss is considered. When an unequal amount of loss is introduced to nanoparticles A and B, the BICs shift along the dispersion band and merge at an off-Γ-point. A remarkable property of the differential loss-induced BIC is that it can be excited by an external plane wave, though it does not radiate itself. Meanwhile, accompanying each BIC, there is a radiative mode located the symmetric place in the Brillouin zone that cannot be excited by the external field. In the end, we consider the case including both gain and loss. Besides the BICs, lasing threshold modes with infinite Q factors can also be supported when the net loss of the system is compensated by the introduced gain. Under certain conditions, the BIC and the lasing threshold mode can be supported simultaneously, resulting in the so-called PT-BICs [40]. Different from the ordinary BIC, the PT-BICs exhibits an anisotropic divergence rate for the total Q factor in the parameter space. The loss-induced BIC and the associated novel properties mentioned can also be extended to other non-Hermitian systems and may find applications in light trapping and lasing.

*yizaomy@swust.edu.cn
†xhong@cqu.edu.cn
‡dzhan@cqu.edu.cn

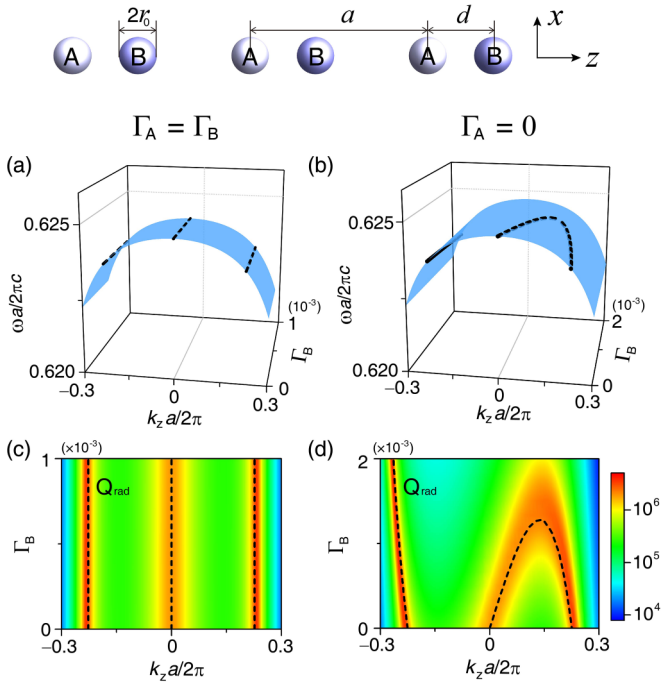

FIG. 1. Evolution of BICs in the dimerized chain with the variation of loss. Upper inset: Schematic of the dimerized chain. Loss can be introduced into nanoparticles A and B separately. (a) and (b) Dispersion of the plasmonic mode with common and differential loss in nanoparticles A and B, respectively. (c) and (d) Simulated radiative Q factors evaluated along the dispersion band correspond to (a) and (b), respectively. The black dashed lines correspond to the analytical result of $P_{\text{rad}} = 0$ according to Eq. (2).

II. THEORY AND RESULTS

We consider an infinite dimerized chain with non-Hermitian perturbation as specified in the upper inset of Fig. 1. There are two plasmonic nanoparticles in a unit cell labeled A and B. The permittivity of each nanoparticle is described by the Drude model, $\varepsilon(\omega) = 1 - \omega_p^2/\omega(\omega + i\gamma_0)$, where ω_p is the plasma frequency and γ_0 is the collision frequency. It is well known that a BIC is characterized by the divergent radiative Q factor because it is decoupled from the far-field radiation [41]. Like previous research on BICs, we ignore the intrinsic loss γ_0 and focus on the radiative loss. In the subwavelength scale $k_0 r_0 \ll 1$ ($k_0 = \omega/c_0$, where c_0 is the light speed in a vacuum), each nanoparticle can be assumed to be an electric dipole with an inverse polarizability $\alpha_0^{-1}(\omega) = \frac{1}{r_0^3}(\frac{\omega_p^2 - 3\omega^2}{\omega_p^2}) - \frac{2i}{3}k_0^3$, where the imaginary part denotes the radiative loss [42]. The non-Hermitian perturbation is introduced by alternating the onsite gain and loss of the A, B nanoparticles. We first consider a purely passive system in which no gain is included. In the theoretical model, the inverse polarizability with loss can now be written as $\alpha_{\text{A}}^{-1}(\omega) = \alpha_0^{-1}(\omega) - i\gamma_{\text{A}}$, and $\alpha_{\text{B}}^{-1}(\omega) = \alpha_0^{-1}(\omega) - i\gamma_{\text{B}}$, where γ_{A} and γ_{B} represent the amounts of loss added to the A and B nanoparticles, respectively. For convenience, the corresponding losses are normalized and represented by Γ_{A} and Γ_{B} with $\Gamma_{\text{A}} = \gamma_{\text{A}} r_0^{-3}$ and $\Gamma_{\text{B}} = \gamma_{\text{B}} r_0^{-3}$.

The linear response for the transverse plasmonic modes (the nanoparticles are y-polarized here) of this non-Hermitian system can be written as [40]

$$\begin{bmatrix} \alpha_0^{-1} - S_{\text{AA}} - i\gamma_{\text{A}} & -S_{\text{AB}} \\ -S_{\text{BA}} & \alpha_0^{-1} - S_{\text{BB}} - i\gamma_{\text{B}} \end{bmatrix} \begin{bmatrix} p_{\text{A}} \\ p_{\text{B}} \end{bmatrix} = \begin{bmatrix} E_{\text{A}} \\ E_{\text{B}} \end{bmatrix}, \quad (1)$$

or in a more compact form: $\mathbf{MP} = \mathbf{E}$, where S_{ij} is the lattice Green's function. Since the resonant states of this system are interested, we set $\mathbf{E} = 0$ in Eq. (1) and look for the complex frequency solutions of $\det(\mathbf{M}) = 0$ for any given k_z, i.e., $\omega(k_z) = \omega'(k_z) + i\omega''(k_z)$. The function $\omega'(k_z)$ gives the dispersion relation of the plasmonic mode, and the ratio $\omega'(k_z)/2\omega''(k_z)$ gives the Q factor. Here, only the zero-order diffraction region, i.e., $|k_z| < \omega/c_0 < 2\pi/a - |k_z|$, is considered.

The linear response in Eq. (1) can also be analyzed by the eigen-decomposition theory via diagonalizing the $\mathbf{M}$ matrix: $\mathbf{MP} = \lambda\mathbf{P}$ [43]. If the corresponding eigenvalue $\lambda = 0$, it will give rise to an eigenstate with a pure real eigenfrequency. For the dimerized chain without gain and loss, the real eigenfrequency states are exactly BICs [7]. When loss is introduced into the system, there cannot exist real eigenfrequency states due to the presence of the net loss. However, states with zero radiation can still exist. Such states are BICs since the field is bound to the structure. To identify the evolution of BICs under the non-Hermitian perturbation, we need to focus on the periodic part of the Bloch wavefunction, which provides significant information [40,44,45]. The matrix $\mathbf{M}$ can be unitarily transformed to $\mathbf{M}' = \mathbf{UMU}$, with $\mathbf{U} = \text{diag}\{e^{ik_z d/2}, e^{-ik_z d/2}\}$. The periodic part of the Bloch wavefunction is then obtained as $\mathbf{P}' = (p'_{\text{A}}, p'_{\text{B}})^{\text{T}} = (p_{\text{A}} e^{ik_z d/2}, p_{\text{B}} e^{-ik_z d/2})^T$. The solution of a BIC must have the form of $\mathbf{P}'_{\text{BIC}} = (1, -1)^T$ to ensure the perfect cancellation of radiation from lattices A and B [7,40]. To reveal the evolution of the BIC, we directly derive the radiation power analytically based on the Green's function method, and the details are given in Supplemental Material Sect. S1 [46]. The radiation power of the dimerized chain in the radial direction is obtained as

$$P_{\text{rad}} = \frac{k_0\left(k_0^2 + k_z^2\right)c_0 |p'_{\text{A}} + p'_{\text{B}}|^2}{16 a \varepsilon_0}, \quad (2)$$

where ε_0 is the vacuum permittivity.

For the dimerized chain shown in the upper inset of Fig. 1, the geometric parameters are set as $r_0 = 20$ nm, $d = 70$ nm, and $a = 230$ nm; and the material parameter is set as $\omega_p = 6.18$ eV. For the plasmonic mode, the inverse of the eigenvalue of the matrix $\mathbf{M}$, $\alpha_{k_z}(\omega) = 1/\lambda_{k_z}(\omega)$ can be regarded as the effective mode polarizability [40]. It has been shown that the locus for the peak of $\text{Im}[\alpha_{k_z}(\omega)]$ or the locus of $\text{Re}[\lambda_{k_z}(\omega)] = 0$ gives the dispersion of the plasmonic modes [7]. For the dimerized plasmonic chain, the dispersion has two branches: the antibonding one and the bonding one [7]. Here, we focus on the bonding mode since it corresponds to the less radiative band.

First we discuss the simple case that common loss is introduced into the nanoparticles A and B, that is, $\Gamma_{\text{A}} = \Gamma_{\text{B}} (\geqslant 0)$. With the increase of loss, the locus of $\text{Re}[\lambda_{k_z}(\omega)] = 0$ shifts accordingly and forms a dispersion band, as indicated by the blue sheet shown in Fig. 1(a). The corresponding radiation power P_{rad} can be calculated analytically by Eq. (2). In the case of no loss, the radiation power P_{rad} drops to zero at

three discrete k_z-points ($k_z = 0, \pm 0.225$), manifesting the existence of three BICs in the dimerized chain. With the increase of the loss strength, the zeros of P_{rad} shift accordingly in the dispersion band, as indicated by the black dashed line in Fig. 1(a). It is worth noting that the locations of k_z for the zeros is unchanged as the symmetry of the system is preserved in this process. For the BICs here, the stored energy decays exponentially in time due to the existence of net loss in the system. To improve the total Q factor of the BICs, gain can be introduced into the systems, as will be discussed later.

Next, we discuss the case of differential loss. For simplicity, the loss in nanoparticle A is fixed as zero and the loss strength in nanoparticles B, Γ_{B}, is a continuous variable. The dispersion of the plasmonic mode with different Γ_{B} is shown by the blue sheet in Fig. 1(b). Strikingly, as Γ_{B} increases, the two BICs with positive k_z move toward each other and then merge into a single BIC at a certain critical value Γ_{B}^c. Above this Γ_{B}^c, the merging BIC disappears and the system is left with only one BIC in the negative k_z space. Because of the breaking of inversion symmetry, the BICs are no longer symmetrically located on the k_z-axis. We will see later that the differential loss leads to peculiar behavior of the BIC, violating the equivalence between zero coupling strength and zero radiative loss.

The analytical results for P_{rad} can be verified numerically by the corresponding Q factors. Figure 1(c) and 1(d) shows the simulated radiative Q factors based on the finite-element method. Here, the radiative Q factor is defined as $Q_{\text{rad}} = \omega(q)U_{\text{eff}}/P_{\text{rad}}$, where U_{eff} is the stored energy and P_{rad} is the radiation power [40,44]. Either for the common loss case or the differential loss case, one can see that the zeros of P_{rad} and the loci of the divergent Q_{rad} factor are highly consistent.

Another notable thing is that the BIC induced by differential loss can be excited by the external plane wave. It is well known that an ordinary BIC cannot radiate, nor can it be excited by an external field [6–8]. However, this is no longer true for the BICs discussed here. The coupling strength between the external field and the eigenstate is defined as $W(k_z,\omega) = \langle\bar{\mathbf{P}}|\mathbf{E}\rangle = \bar{p}_{\text{A}}E_{\text{A}} + \bar{p}_{\text{B}}E_{\text{B}}$ [40,47]. Here, $|\mathbf{E}\rangle$ is the external field and $\langle\bar{\mathbf{P}}|$ is the left eigenvector of matrix $\mathbf{M}$ in Eq. (1). Due to the symmetry properties of $\mathbf{M}$, i.e., $\mathbf{M}(-k_z,\omega) = \mathbf{M}^{\text{T}}(k_z,\omega)$, it is easy to show that the left eigenvector at k_z shares the same entries with the right eigenvector at $-k_z$, namely, $\langle\bar{\mathbf{P}}|_{k_z} = |\mathbf{P}\rangle^T_{-k_z}$. Considering a plane-wave incidence with $|\mathbf{E}\rangle \propto (e^{-ik_z d/2}, e^{ik_z d/2})^T$ and defining $|\mathbf{P}\rangle = (p_{\text{A}}, p_{\text{B}})^T \overset{\text{def}}{=} (p'_{\text{A}}e^{-ik_z d/2}, p'_{\text{B}}e^{ik_z d/2})^T$, we have $W(k_z,\omega) \propto \bar{p}_{\text{A}}(k_z)e^{-ik_z d/2} + \bar{p}_{\text{B}}(k_z)e^{ik_z d/2} = p'_{\text{A}}(-k_z) + p'_{\text{B}}(-k_z)$.

Figure 2 shows the calculated $W(k_z, \omega)$, both the absolute value and phase, along the dispersion of the plasmonic mode. The trajectories of the BICs extracted from Fig. 1(b) are also shown, as indicated by the black dashed lines. One can see that $W(k_z, \omega)$ drops to zero continuously at the place where a phase jump of π takes place, as shown in Fig. 2(b). Apparently, the trajectories of the BICs are not coincident with those of the zero coupling strength states. Actually, they are symmetric with each other. Thus, the BICs can be excited by an external field since the corresponding $W(k_z, \omega) \neq 0$, except when $\Gamma_{\text{B}} = 0$. In the case of $\Gamma_{\text{B}} = 0$, where both gain and loss are absent, the BICs locate at the zero points of

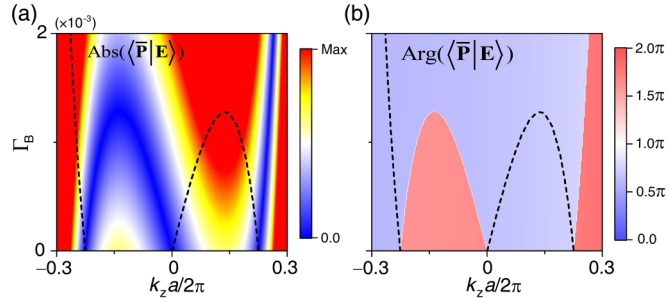

FIG. 2. Coupling strength $W(k_z, \omega)$ of the bonding mode. (a) and (b) The absolute value and phase of $W(k_z, \omega)$, respectively. $W(k_z, \omega)$ drops to zero at the place where a π phase jump happens. The trajectories of BICs are indicated by the dashed black lines where $W(k_z, \omega) \neq 0$ except when $\Gamma_{\text{B}} = 0$.

$W(k_z, \omega)$, indicating they cannot be excited by the external field. Such ordinary BICs have been investigated in detail in previous work [7].

The radiation and excitation properties of these peculiar states can be described in a figurative way. The ordinary BICs can be described as "deaf-mute modes" since they can neither be excited by external waves nor can they radiate to infinity. The differential loss-induced BICs can then be described as "mute but not deaf modes" as they do not radiate but can be excited. However, for the zero coupling strength states, they are "deaf but not mute modes" because they can radiate but cannot be excited. It should be noted that these peculiar states, both the "mute but not deaf mode" and "deaf but not mute mode" are completely different from the quasi-BICs, which are ordinary BICs with compromised Q factors due to symmetry breaking or a finite-size structure [16,48,49]. In fact, the quasi-BIC can radiate and also can be excited by waves coming from the far field.

The afore-mentioned excitation behaviors can be explained analytically. When $\Gamma_{\text{B}} = 0$, the system is inversion symmetric and $W(k_z, \omega) = W(-k_z, \omega)$. It is guaranteed that the BICs are symmetrically distributed and the corresponding $W(k_z, \omega) = 0$, that is, they cannot be excited. With the increase of Γ_{B}, the inversion symmetry is broken. Note that the right eigenvector of a BIC always has the antisymmetric form, i.e., $\mathbf{P}'_{\text{BIC}} = (1, -1)^T$, but the left and right eigenvectors of a loss-induced BIC have different entries due to the influence of non-Hermitian components [40]. Meanwhile, as mentioned previously, we have $\langle\bar{\mathbf{P}}|_{k_z} = |\mathbf{P}\rangle^T_{-k_z}$. Therefore, the coupling strength, $W(k_z,\omega) \propto (p'_{\text{A}} + p'_{\text{B}})_{-k_z}$, does not vanish at the BICs. In contrast, accompanying the BIC at $k_{z,\text{BIC}}$, the state at $-k_{z,\text{BIC}}$ has the coupling strength $W(-k_{z,\text{BIC}},\omega) \propto (p'_{\text{A}} + p'_{\text{B}})_{k_{z,\text{BIC}}} = 0$. Thus, the trajectories of the BICs and the zero coupling strength states are symmetric with each other. In this sense, the evolution shown in Fig. 2 can be described as a splitting and merging process: the original BIC (deaf-mute mode) splits into a "mute but not deaf mode" and a "deaf but not mute mode," then two "mute but not deaf modes" and two "deaf but not mute modes" merge and disappear separately.

To demonstrate the previously mentioned asymmetric behavior further, the response of the system to an external field is

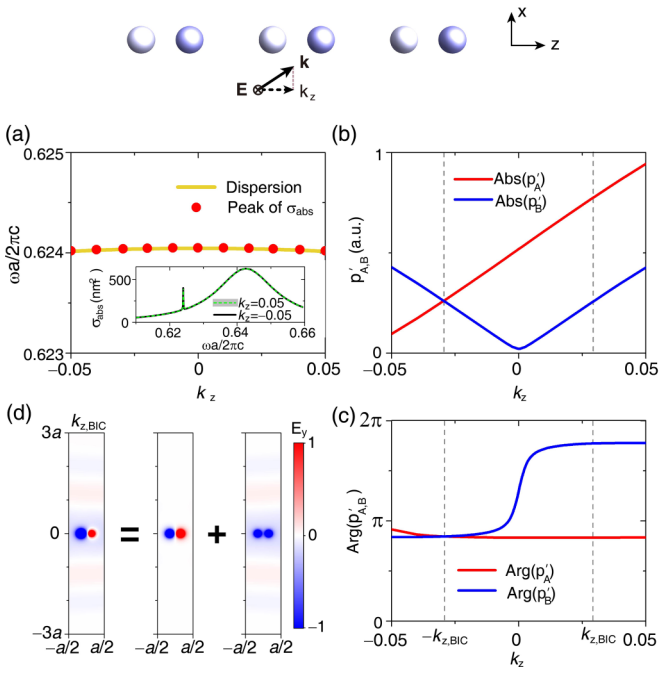

FIG. 3. Excitation of the dimerized chain by an external plane wave. The system is illuminated by a plane wave, as illustrated by the upper inset. (a) Dispersion of the resonant mode obtained from the simulation (yellow line) and the frequencies of the peaks for the absorption cross section σ_{abs} (red circles). The inset shows σ_{abs} corresponding to $k_z = \pm 0.05$. (b) and (c) The absolute values and phases of the excited dipole moments at the peaks of σ_{abs}, respectively. The zero-coupling strength state and BIC are indicated by the dash lines at $-k_{z,\mathrm{BIC}}$ and $k_{z,\mathrm{BIC}}$, respectively. (d) Decomposition of the field profiles (E_y) at $k_{z,\mathrm{BIC}}$ into the antisymmetric component and the symmetric component.

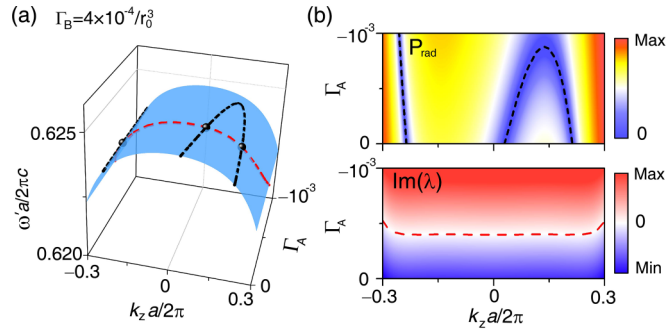

FIG. 4. BICs and lasing threshold modes in the dimerized chain with both gain and loss. (a) The dispersion band (blue sheet) of the plasmonic mode under different gain. Here, the loss in nanoparticle B is fixed as $\Gamma_B = 4 \times 10^{-4}$. (b) The radiating power P_{rad} (upper panel) and the imaginary part of the eigenvalue (lower panel) of the plasmonic modes. The black dashed lines and the red dashed line are the corresponding nodal lines, indicating the BICs and the lasing threshold modes, respectively. The three crossing points [black dots in (a)] of the two nodal lines give rise to the *PT*-BICs.

numerically simulated. As shown in the upper inset of Fig. 3, the system is illuminated by a *y*-polarized plane wave. Here, the loss is set as $\Gamma_A = 0$ and $\Gamma_B = 4 \times 10^{-4}$. As an example, the absorption cross section σ_{abs} corresponding to $k_z = \pm 0.05$ is calculated as shown in the inset of Fig. 3(a) and two peaks can be observed. The sharp peak with a lower frequency corresponds to the bonding mode and the broad peak with a higher frequency corresponds to the antibonding mode. The peaks of σ_{abs} for the bonding mode, as indicated by the red dots, are shown in Fig. 3(a), with excellent agreement with the dispersion of the plasmonic mode. The absolute value and the corresponding phase of excited dipole moments $p'_{A,B}$ at the peaks of σ_{abs} are calculated and shown in Fig. 3(b) and (c), respectively. Apparently, the response of the system is asymmetric along the k_z-axis. This asymmetry can be further confirmed by the corresponding field profiles of the system when illuminated by a plane wave with a different incident angle. In fact, this asymmetry can also be reflected by the corresponding eigen fields. More details about the profiles are presented in Supplemental Material Sect. S2 [46]. According to the numerically obtained Q factor shown in Fig. 1(d), a BIC is located at $k_z = 0.029$ in the bonding band. And the state at $k_z = -0.029$ corresponds to the "deaf but not mute state" that cannot be excited. The excited dipole moments p'_A and p'_B at $k_z = -0.029$ are numerically identical. This excitation is purely from the background of the antibonding mode, which is dominated by the symmetric mode with the form of $\mathbf{P}' = (1,1)^T$. As for the excitation at $k_z = 0.029$, both the symmetric and antisymmetric modes are excited, and the ratio of the corresponding amplitudes is about 1:2. As shown in Fig. 3(d), the field profile at $k_z = 0.029$ is decomposed into an antisymmetric component and a symmetric component. Note that the background coming from the antibonding mode is almost a pure symmetric mode; the antisymmetric component observed at $k_z = 0.029$ is coming from the bonding mode, manifesting the excitation of BIC.

In the end, we consider the case with both gain and loss involved. For simplicity, the loss of nanoparticle B is fixed as $\Gamma_B = 4 \times 10^{-4}$ and the gain of nanoparticle A is a variable. Here, $\Gamma_A < 0$, representing the gain added to nanoparticle A. The dispersion of the system with different gain is shown in Fig. 4(a), as indicated by the blue sheet. The corresponding radiation power P_{rad} is shown in the upper panel of Fig. 4(b), with the dashed lines indicating $P_{rad} = 0$, namely, the BICs. With the increase of $|\Gamma_A|$, the two BICs in positive k_z space move toward each other, then merge together and finally disappear.

The lower panel of Fig. 4(b) shows the imaginary part of the eigenvalue, Im(λ). The red dashed line is the nodal line of Im(λ), on which both Im(λ) and Re(λ) equal zero, giving the lasing threshold mode with real eigenfrequency. The trajectories of the lasing threshold mode and BICs, as marked in Fig. 4(a), intersect at three points, giving rise to the nonradiative states with real eigenfrequency, namely the so-called *PT*-BICs. Strictly speaking, an optical system can have PT symmetry at isolated frequency points only due to the dispersion of the permittivity [50,51]. For the *PT*-BICs here, they locate in a very narrow frequency range, hence the PT-symmetry condition holds well approximately.

It is worth noting that unphysical effects may happen for the *PT*-BICs in the frame of linear optics. At the *PT*-BICs, the energy stored in the system will keep growing with time when illuminated, as they can be excited by external waves but

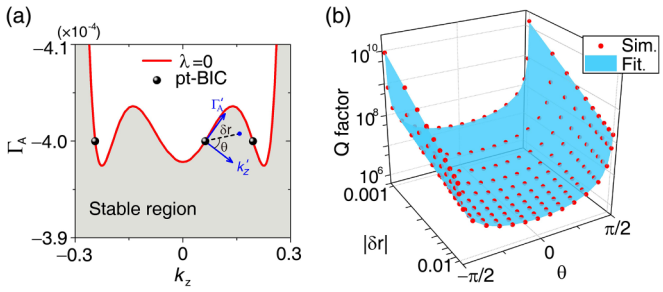

FIG. 5. Behavior of Q factors near a PT-BICs. (a) The zoom-in view of the k_z-Γ_A space, including the lasing threshold modes (red line) and PT-BICs (black dots) shown in Fig. 4. The normal (k'_z) and tangent (Γ'_A) of the red line at the PT-BICs are defined as the axes of the local coordinate system. A point near the PT-BICs is specified by δr and θ. (b) The Q factors for the resonant states near the PT-BICs in the stable region. The Q-factor divergence rate relies on the angle θ and can be well fitted by the function $[k'_z + c\Gamma'^2_A]^{-1}$, as shown by the blue sheet.

do not radiate, leading to energy divergence. This unphysical effect results from the assumption that the system remains linear at high power, which is not true for the real situation. At high light intensity, nonlinear effect such as second- or third-harmonic generation will appear and give rise to radiation, hence energy divergence will not happen.

It worth noting that the PT-BICs exhibit an anisotropic Q-factor divergence behavior in the parameter space. Figure 5(a) is the zoom-in view of the k_z-Γ_A space in which the lasing threshold modes (red lines) and PT-BICs (black dots) shown in Fig. 4 are presented. The nodal line of $\lambda = 0$ divides the k_z-Γ_A parameter space into the stable passive region and the unstable lasing region, and we are concerned with the Q factors in the stable region. We take the PT-BICs at the point $(k_z,\ \Gamma_A) = (0.0625,\ -4 \times 10^{-4})$ as an example. For convenience, we set a local coordinate system as shown in Fig. 5(a). At the PT-BICs point, the normal (k'_z) and tangent (Γ'_A) of the red line ($\lambda = 0$) are defined as the two coordinate axes in Fig. 5(a). A point near the PT-BICs is specified by the distance δr from the PT-BICs point and the position angle θ with respect to the k'_z-axis. Then the Q factors for the points near the PT-BICs are calculated and shown in Fig. 5(b), as indicated by the red dots. When $\theta = 0$, the Q factor diverges at a rate of k'^{-1}_z. When $\theta = \pi/2$, the Q factor diverges in the form of Γ'^{-2}_A. Thus, a generic form of the Q-factor divergence rate can be written as $[k'_z + c\Gamma'^2_A]^{-1}$, where c is a constant. The fitted result is shown in Fig. 5(b) by the blue surface, which agrees well with the calculated results. The anisotropic Q-factor divergence rate of the PT-BICs is rather different from the previously reported behavior of $Q \propto \delta k^{-2}$ [6,11,12,18] or $Q \propto [\delta k_x + c\delta k_y^2]^{-1}$ [44]. Moreover, like loss-induced BIC, PT-BICs also possesses the property that it can be excited by an external field as shown in Supplemental Material Sect. S2 [46].

III. CONCLUSION

In summary, we have demonstrated the evolution and the peculiar properties of the BICs under a non-Hermitian perturbation. When differential loss is introduced into the system, the inversion symmetry of the system is broken, resulting in the asymmetric behavior of the loss-induced BIC. The original BIC split into a nonradiative state (BIC) and a zero-coupling strength state. Different from ordinary BICs, the loss-induced BICs can be excited by an external plane wave, although they do not radiate. On the contrary, the zero-coupling strength states cannot be excited by a plane wave, although they can radiate. When both gain and loss are included in the system, lasing threshold modes can be supported if the net loss is exactly balanced by the gain. The lasing threshold mode and the BIC can exist simultaneously, forming a PT-BICs. The PT-BICs carries an anisotropic Q-factor divergence rate in the parameter space, which is very different from the ordinary BIC. These characteristics can be implemented in other optical systems and may offer new perspective to BICs in a non-Hermitian system.

ACKNOWLEDGMENTS

This work was supported by the National Natural Science Foundation of China (Grants No. 12204388, No. 12074049 and No. 12147102), the Natural Science Foundation of Sichuan Province (Grant No. 2022NSFSC1804), the Scientific Research Fund of Sichuan Provincial Science and Technology Department (Grant No. 2020YJ0137), the Fundamental Research Funds for the Central Universities (Grant No. 2022CDJQY-007), and the Doctor Foundation of Southwest University of Science and Technology (Grant No. 21zx7141).

[1] J. von Neumann and E. Wigner, Über merkwürdige diskrete Eigenwerte, Phys. Z. **30**, 465 (1929).
[2] H. Friedrich and D. Wintgen, Interfering resonances and bound states in the continuum, Phys. Rev. A **32**, 3231 (1985).
[3] E. N. Bulgakov and A. F. Sadreev, Formation of bound states in the continuum for a quantum dot with variable width, Phys. Rev. B **83**, 235321 (2011).
[4] S. W. Dai, L. Liu, D. Z. Han, and J. Zi, From topologically protected coherent perfect reflection to bound states in the continuum, Phys. Rev. B **98**, 081405(R) (2018).
[5] X. Gao, C. W. Hsu, B. Zhen, X. Lin, J. D. Joannopoulos, M. Soljačić, and H. Chen, Formation mechanism of guided resonances and bound states in the continuum in photonic crystal slabs, Sci. Rep. **6**, 31908 (2016).
[6] E. N. Bulgakov and D. N. Maksimov, Topological Bound States in the Continuum in Arrays of Dielectric Spheres, Phys. Rev. Lett. **118**, 267401 (2017).
[7] Q. J. Song, M. Zhao, L. Liu, J. Chai, G. He, H. Xiang, D. Z. Han, and J. Zi, Observation of bound states in the continuum in the dimerized chain, Phys. Rev. A **100**, 023810 (2019).
[8] C. W. Hsu, B. Zhen, A. D. Stone, J. D. Joannopoulos, and M. Soljačić, Bound states in the continuum, Nat. Rev. Mater. **1**, 16048 (2016).

[9] B. Zhen, C. W. Hsu, L. Lu, A. D. Stone, and M. Soljačić, Topological Nature of Optical Bound States in the Continuum, Phys. Rev. Lett. **113**, 257401 (2014).
[10] T. Yoda and M. Notomi, Generation and Annihilation of Topologically Protected bound States in the Continuum and Circularly Polarized States by Symmetry Breaking, Phys. Rev. Lett. **125**, 053902 (2020).
[11] J. Jin, X. Yin, L. Ni, M. Soljačić, B. Zhen, and C. Peng, Topologically enabled ultrahigh-Q guided resonances robust to out-of-plane scattering, Nature (London) **574**, 501 (2019).
[12] M. Kang, S. Zhang, M. Xiao, and H. Xu, Merging Bound States in the Continuum at Off-High Symmetry Points, Phys. Rev. Lett. **126**, 117402 (2021).
[13] B. Wang, W. Liu, M. Zhao, J. Wang, Y. Zhang, A. Chen, F. Guan, X. Liu, L. Shi, and J. Zi, Generating optical vortex beams by momentum-space polarization vortices centred at bound states in the continuum, Nat. Photon. **14**, 623 (2020).
[14] C. Huang, C. Zhang, S. Xiao, Y. Wang, Y. Fan, Y. Liu, N. Zhang, G. Qu, H. Ji, J. Han, L. Ge, Y. Kivshar, and Q. Song, Ultrafast control of vortex microlasers, Science **367**, 1018 (2020).
[15] M. Zhang and X. D. Zhang, Ultrasensitive optical absorption in graphene based on bound states in the continuum, Sci. Rep. **5**, 8266 (2015).
[16] Z. Liu, Y. Xu, Y. Lin, J. Xiang, T. Feng, Q. Cao, J. Li, S. Lan, and J. Liu, High-Q Quasibound States in the Continuum for Nonlinear Metasurfaces, Phys. Rev. Lett. **123**, 253901 (2019).
[17] Y. X. Xiao, G. C. Ma, Z. Q. Zhang, and C. T. Chan, Topological Subspace-Induced Bound State in the Continuum, Phys. Rev. Lett. **118**, 166803 (2017).
[18] L. Yuan and Y. Y. Lu, Bound states in the continuum on periodic structures surrounded by strong resonances, Phys. Rev. A **97**, 043828 (2018).
[19] X. Wang, J. Duan, W. Chen, C. Zhou, T. Liu, and S. Y. Xiao, Controlling light absorption of graphene at critical coupling through magnetic dipole quasi-bound states in the continuum resonance, Phys. Rev. B **102**, 155432 (2020).
[20] Ş. K. Özdemir, S. Rotter, F. Nori, and L. Yang, Parity-time symmetry and exceptional points in photonics, Nat. Mater. **18**, 783 (2019).
[21] R. El-Ganainy, K. G. Makris, M. Khajavikhan, Z. H. Musslimani, S. Rotter, and D. N. Christodoulides, Non-Hermitian physics and PT symmetry, Nat. Phys. **14**, 11 (2018).
[22] L. Feng, R. El-Ganainy, and L. Ge, Non-Hermitian photonics based on parity-time symmetry, Nat. Photon. **11**, 752 (2017).
[23] M. A. Miri and A. Alù, Exceptional points in optics and photonics, Science **363**, eaar7709 (2019).
[24] C. A. Valagiannopoulos, F. Monticone, and A. Alù, PT-symmetric planar devices for field transformation and imaging, J. Opt. **18**, 044028 (2016).
[25] A. Krasnok, N. Nefedkin, and A. Alù, Parity-time symmetry and exceptional points, IEEE Antenn. Propag. M **63**, 110 (2021).
[26] C. M. Bender and S. Boettcher, Real Spectra in Non-Hermitian Hamiltonians Having PT Symmetry, Phys. Rev. Lett. **80**, 5243 (1998).
[27] B. Peng, Ş. K. Özdemir, F. Lei, F. Monifi, M. Gianfreda, G. L. Long, S. Fan, F. Nori, C. M. Bender, and L. Yang, Parity-time symmetric whispering-gallery microcavities, Nat. Phys. **10**, 394 (2014).
[28] A. Guo, G. J. Salamo, D. Duchesne, R. Morandotti, M. Volatier-Ravat, V. Aimez, G. A. Siviloglou, and D. N. Christodoulides, Observation of PT-symmetry Breaking in Complex Optical Potentials, Phys. Rev. Lett. **103**, 093902 (2009).
[29] L. Feng, Y. L. Xu, W. S. Fegadolli, M. H. Lu, J. E. Oliveira, V. R. Almeida, and A. Scherer, Experimental demonstration of a unidirectional reflectionless parity-time metamaterial at optical frequencies, Nat. Mater. **12**, 108 (2013).
[30] Y. L. Xu, W. S. Fegadolli, L. Gan, M. H. Lu, X. P. Liu, Z. Y. Li, and Y. F. Chen, Experimental realization of Bloch oscillations in a parity-time synthetic silicon photonic lattice, Nat. Commun. **7**, 11319 (2016).
[31] L. Feng, Z. J. Wong, R. M. Ma, Y. Wang, and X. Zhang, Single-mode laser by parity-time symmetry breaking, Science **346**, 972 (2014).
[32] H. Hodaei, M. A. Miri, M. Heinrich, D. N. Christodoulides, and M. Khajavikhan, Parity-time symmetric microring lasers, Science **346**, 975 (2014).
[33] B. Zhen, C. W. Hsu, Y. Igarashi, L. Lu, I. Kaminer, A. Pick, and M. Soljačić, Spawning rings of exceptional points out of Dirac cones, Nature (London) **525**, 354 (2015).
[34] Y. Zhiyenbayev, Y. Kominis, C. Valagiannopoulos, V. Kovanis, and A. Bountis, Enhanced stability, bistability, and exceptional points in saturable active photonic couplers, Phys. Rev. A **100**, 043834 (2019).
[35] Y. Kominis, V. Kovanis, and T. Bountis, Controllable asymmetric phase-locked states of the fundamental active photonic dimer, Phys. Rev. A **96**, 043836 (2017).
[36] D. V. Novitsky, A. S. Shalin, D. Redka, V. Bobrovs, and A. V. Novitsky, Quasibound states in the continuum induced by PT symmetry breaking, Phys. Rev. B **104**, 085126 (2021).
[37] W. Chen, Ş. K. Özdemir, G. Zhao, J. Wiersig, and L. Yang, Exceptional points enhance sensing in an optical microcavity, Nature (London) **548**, 192 (2017).
[38] K. Ding, G. Ma, M. Xiao, Z. Q. Zhang, and C. T. Chan, Emergence, Coalescence, and Topological Properties of Multiple Exceptional Points and Their Experimental Realization, Phys. Rev. X **6**, 021007 (2016).
[39] W. Zhu, X. Fang, D. Li, Y. Sun, Y. Li, Y. Jing, and H. Chen, Simultaneous Observation of a Topological Edge State and Exceptional Point in an Open and Non-Hermitian Acoustic System, Phys. Rev. Lett. **121**, 124501 (2018).
[40] Q. J. Song, J. Hu, S. Dai, C. Zheng, D. Han, J. Zi, Z. Q. Zhang, and C. T. Chan, Coexistence of a new type of bound state in the continuum and a lasing threshold mode induced by PT symmetry, Sci. Adv. **6**, eabc1160 (2020).
[41] C. W. Hsu, B. Zhen, J. Lee, S. L. Chua, S. G. Johnson, J. D. Joannopoulos, and M. Soljačić, Observation of trapped light within the radiation continuum, Nature (London) **499**, 188 (2013).
[42] W. H. Weber and G. W. Ford, Propagation of optical excitations by dipolar interactions in metal nanoparticle chains, Phys. Rev. B **70**, 125429 (2004).
[43] K. H. Fung and C. T. Chan, Plasmonic modes in periodic metal nanoparticle chains: A direct dynamic eigenmode analysis, Opt. Lett. **32**, 973 (2007).
[44] Q. J. Song, S. Dai, D. Z. Han, Z. Q. Zhang, C. T. Chan, and J. Zi, PT symmetry induced rings of lasing threshold modes embedded with discrete bound states in the continuum, Chin. Phys. Lett. Express Letter **38**, 84203 (2021).

[45] W. Chen, Y. Chen, and W. Liu, Singularities and Poincaré Indexes of Electromagnetic Multipoles, Phys. Rev. Lett. **122**, 153907 (2019).

[46] See Supplemental Material at http://link.aps.org/supplemental/10.1103/PhysRevB.107.165142 for an estimation of radiation and absorption by Green's function, asymmetric behavior of the field profiles in momentum space, and the coupling of *PT*-BICs to an external field.

[47] V. A. Markel, Antisymmetrical optical states, J. Opt. Soc. Am. B **12**, 1783 (1995).

[48] P. Zheng, P. Raj, T. Mizutani, M. Szabo, W. A. Hanson, and I. Barman, Plexcitonic quasi-bound states in the continuum, Small **17**, 2102596 (2021).

[49] A. Taghizadeh and I. S. Chung, Quasi bound states in the continuum with few unit cells of photonic crystal slab, Appl. Phys. Lett. **111**, 031114 (2017).

[50] A. A. Zyablovsky, A. P. Vinogradov, A. V. Dorofeenko, A. A. Pukhov, and A. A. Lisyansky, Causality and phase transitions in PT-symmetric optical systems, Phys. Rev. A **89**, 033808 (2014).

[51] F. A. Shuklin, C. Tserkezis, N. A. Mortensen, and C. Wolff, Fundamental issues with light propagation through PT-symmetric systems, Phys. Rev. A **105**, 053527 (2022).